Reprinted from THE JOURNAL OF CHEMICAL PHYSICS, Vol. 45, No. 5, 1723–1732, 1 September 1966
Printed in U. S. A.

Atom–Atom Ionization Cross Sections of the Noble Gases—Argon, Krypton, and Xenon*

ARNOLD J. KELLY†
Daniel and Florence Guggenheim Jet Propulsion Center, Karman Laboratory of Fluid Mechanics and Jet Propulsion
California Institute of Technology, Pasadena, California

(Received 18 April 1966)

An experimental investigation of the initial phase of shock produced ionization in argon, krypton, and xenon has been conducted in order to elucidate the atom–atom ionization reaction and to determine the atom–atom ionization cross sections. A high-purity shock tube was employed to heat these gases to temperatures in the range from 5000° to 9000°K at neutral particle densities of 4.4×10^{17}, 7.0×10^{17}, and 13.3×10^{17} cm^{-3}, and impurity levels of approximately 10^{-6}. A K-band (24-GHz) microwave system situated so that the microwave-beam propagation direction was normal to the shock tube, monitored the ionization relaxation process occurring immediately after the passage of the shock front. Electron density was calculated from the microwave data using a plane-wave–plane-plasma slab interaction theory corrected for near field effects associated with the coupling of the microwave energy to the plasma. These data, adjusted to compensate for the effects of shock attenuation, verified that the dominant electron-generation process involve a two-step, atom–atom ionization reaction, the first step (excitation to the first excited states) being rate determining. The quadratic dependence on neutral density associated with this reaction was experimentally demonstrated (with an uncertainty of ±15%). The cross section, characterized as having a constant slope from threshold (first excited energy level), represented as the cross-sectional slope constant C, was found to be equal to $1.2\times10^{-19}\pm15\%$ cm^2/eV, $1.4\times10^{-19}\pm15\%$ cm^2/eV, and $1.8\times10^{-20}\pm15\%$ cm^2/eV for argon, krypton, and xenon, respectively. The electron–atom elastic momentum-exchange cross sections derived from the microwave data correlated quite well with Maxwell-averaged beam data, the agreement for the case of argon being ±20%; krypton, ±30%; and xenon, within a factor of 2.

INTRODUCTION

THERMAL ionization processes in the gas phase proceed by electron–atom ionization[1–3] except when the electron concentration is very low. This latter situation occurs when a volume of gas is heated rapidly by a shock wave of sufficient strength to produce a sensible level of ionization in the equilibrium state. Neglecting photoionization[4,5] and electron diffusion from highly ionized zones,[6] the electrons must be generated through atom–atom interaction until the electron concentration has reached the level where the faster atom–electron reaction becomes dominant. Until this time, however, the atom–atom process is the rate-controlling step.

The results of Petschek and Byron[1] indicated that the initial (atom–atom) ionization in argon proceeds by a two-step mechanism, the first rate-controlling step of which is associated with the first atomic excitation level, a conclusion which was substantiated by Weymann.[6] In these experiments, the delay time between shock passage and the occurrence of luminosity was observed, the onset of luminosity being attributed to electron–atom ionization. Employing the techniques of microwave absorption, Johnston and Kornegay[7] were apparently first to demonstrate clearly that the atom–atom ionization of xenon proceeds by a two-step process, the rate-controlling first step of which has an activation-energy equivalent to the first excited atomic level.

Recently, Harwell and Jahn,[8] employing a transverse microwave probe in the study of shock-heated argon, krypton, and xenon, demonstrated that in each case the atom–atom ionization involved a two-step process, the activation energy of the first step corresponding to that of the first atomic energy level. The profound effects of very small impurity levels, examined critically in Refs. 3 and 8, limited the detail with which conclusions could be drawn from these data. Consequently, the quadratic pressure dependence of ionization rate, demanded by the proposed mechanism, could only be qualitatively indicated.

In the present work, this line of experimentation, initiated by Jahn, is continued at what is believed to be a purity level an order of magnitude better than that achieved in Ref. 8. The results permit accurate determination of the ionization cross sections for the three noble gases, provide a conclusive check on the quadratic dependence of ionization rate upon pressure, and give considerably improved values for the absolute ionization rates.

* Supported by the U.S. Air Force Office of Scientific Research under Contract AF 49(638)-1285.

† Graduate Student; now Senior Research Engineer, Jet Propulsion Laboratory, Pasadena, Calif.

[1] H. E. Petschek and S. Byron, Ann. Phys. (N.Y.) **1**, 270 (1957).

[2] L. M. Biberman and I. T. Yakubov, Soviet Phys.—Tech. Phys. **8**, 1001 (1964) [Zh. Tekhn. Fiz. **33**, 1344 (1963)].

[3] E. J. Morgan and R. D. Morrison, Phys. Fluids **8**, 1608 (1965).

[4] T. Holstein, Phys. Rev. **72**, 1212 (1947).

[5] J. H. Clarke and C. Ferrari, Phys. Fluids **8**, 2121 (1965).

[6] H. D. Weymann, "On the Mechanism of Thermal Ionization Behind Strong Shock Waves," University of Maryland Tech. Note BN-144 (1958).

[7] (a) H. S. Johnston and W. M. Kornegay, Trans. Faraday Soc. **57**, 1563 (1961); (b) W. M. Kornegay and H. S. Johnston, J. Chem. Phys. **38**, 2242 (1963).

[8] K. E. Harwell and R. G. Jahn, Phys. Fluids **7**, 214 (1964).

TABLE I. Activation energies and cross-sectional slope constants.

Species	P_1(torr)[a]	E_*(eV)	C(cm²/eV)[b]
Argon	3	11.8±1.1	1.15×10^{-19}
	5	11.2±0.9	1.24×10^{-19}
	10	11.4±1.0	1.04×10^{-19}
Krypton	3	9.6±0.9	1.68×10^{-19}
	5	10.1±0.7	1.29×10^{-19}
	10	10.1±0.7	1.32×10^{-19}
Xenon	5	8.2±0.7	1.90×10^{-20}
	10	8.4±0.7	1.66×10^{-20}

[a] 3, 5, and 10 torr are equivalent to particle densities of 4.41×10^{17} cm^{-3}, 6.96×10^{17} cm^{-3}, and 13.26×10^{17} cm^{-3}, respectively.
[b] Reduced on the basis of: $E_{*Ar}=11.548$ eV, $E_{*Kr}=9.915$ eV, $E_{*Xe}=8.315$ eV.

THE TWO-STEP ATOM-ATOM IONIZATION PROCESS

The two-step, atom–atom excitation and ionization is assumed to proceed according to the equations

$$A+A\rightarrow A+A^* \quad \text{excitation,} \qquad (1a)$$

$$A+A^*\rightarrow A+A^++e \quad \text{ionization,} \qquad (1b)$$

where A* represents an excited state and A^+ the ion. In the noble gases (Ar, Kr, Xe), for moderate pressures (200→800 torr) and temperatures (0.45→0.85 eV), the first step in the reaction results in the elevation of one of the collision partners to one of the four closely spaced energy levels comprising the first excited state. Two of these levels are energetically isolated from the ground state, i.e., they are metastable. Transitions between the other two levels and the ground state are permitted by the selection rules and give rise to the so-called resonance radiation. If collisionally excited into one of the metastable states, the atom could remain in that state for time periods of the order of 10^{-4} sec[9] because of its inability to radiate the ground state. The probability that a second inelastic collision would occur leading to ionization of this atom is consequently greatly enhanced. This second collision need only supply a fraction of the energy required for the initial excitation to cause ionization. In the case of argon, 11.55 eV is necessary for excitation (lowest metastable state), but only an additional 4.21 eV is required for ionization from this state. Were the atom collisionally excited to one of the resonance levels which, for the noble gases studied, lie <0.3 eV above the lowest metastable level, radiative decay would occur in on the order of 10^{-8} sec. However, since the gas is optically thick for this resonance radiation, the emitted photon will be trapped in the gas,[4] individual atoms being alternately collisionally or radiatively excited and radiatively de-excited, and the over-all population would remain relatively constant. Therefore, the probability of an inelastic atom–atom collision occurring when one of the collision partners is in an excited state will be vastly increased over that in the absence of resonance radiation trapping.

Because the metastable states lie somewhat below the resonance levels, the Boltzmann probability factor for a reaction involving the metastable state is higher than for those involving the resonance states. However, the difference in energy separating these state is commensurate with the experimental uncertainty associated with the determination of these energies, cf. Table I. Therefore, it is currently not possible to ascertain which of these two mechanisms, i.e., excitation of the long-lived metastable states or resonance radiation trapping, is dominant, or indeed, if they are independent. One can only state that the two-step ionization process has been established as the preferred atom–atom ionization path, that the first step of this process is the rate-controlling step, and that collisional and radiative de-excitation and recombination have a negligible effect upon the population of the excited state. Consequently, the cross sections determined for these reactions are in actuality not truly ionization cross sections but rather those of the rate-controlling excitation reaction.

ATOM–ATOM ELECTRON-GENERATION RATES

For a single species gas undergoing atom–atom ionization, the ionization rate (i.e., rate of excitation) can be written as

$$\tfrac{1}{2}(N_a^2)CK(1/\beta)^{3/2}(2+\beta E_*)\exp(-\beta E_*), \qquad (2)$$

where N_a is the neutral-particle density [C the cross-sectional scope constant which is related to the cross section Q by the relation $Q=C(E-E_*)$], E_* is the threshold reaction energy, β is $1/kT$, and $K\equiv(2\sqrt{2})/(\mu\pi)^{1/2}$, μ being the reduced mass of the reactant atoms. In the absence of negative ion formation in the noble gases, over all neutrality of the gas implies that the rate of excitation expressed by Eq. (2) is identical to the rate of electron generation per unit volume.

As discussed in Ref. 8, there is a preliminary phase associated with the two-step ionization process. During this phase, the first excited states are being populated and the electron density will be expected to exhibit a cubic dependence in neutral-particle density and a quadratic dependence on time. During this period the electron density is below the threshold of the present experiments and will not be observed. Consequently, Eq. (2) should be the appropriate description of the observations on the atom–atom excitation–ionization process.

SHOCK-TUBE DESIGN

A schematic drawing of the over-all shock tube used in these experiments is shown in Fig. 1. The tube itself

[9] A. C. G. Mitchell and M. W. Zemansky, *Resonance Radiation and Excited Atoms* (Cambridge University Press, New York, 1961).

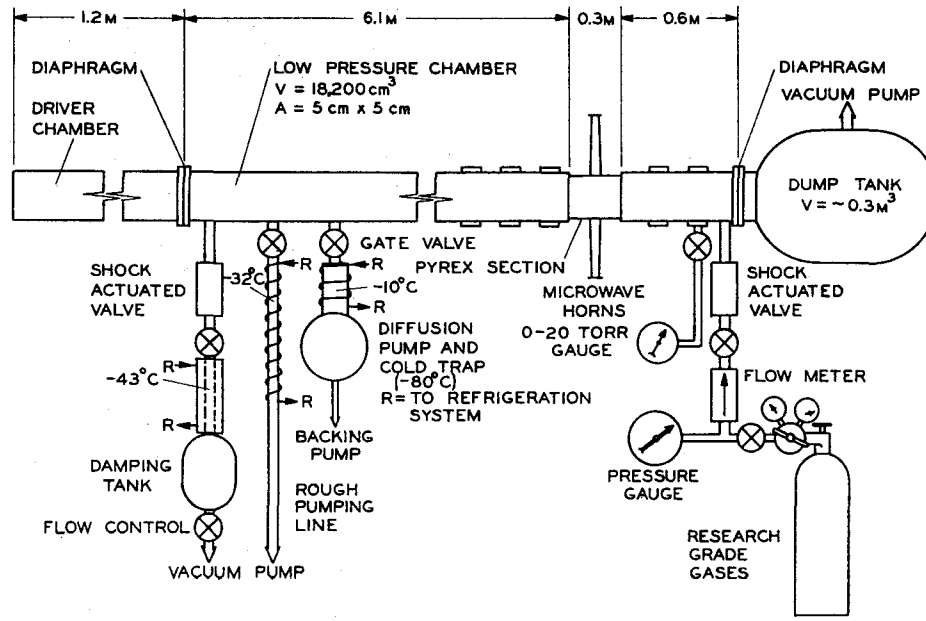

FIG. 1. Schematic of shock tube and flow system.

was constructed of 6066–T5 aluminum tubing having a square internal passage 5 cm by 5 cm. All sections of the tube were sealed with standard Buna N O-rings which were adequate to permit evacuation to pressure levels of approximately 2×10^{-6} torr. The driver section, consisting of a 1.2-m length of tubing, permitted driver pressures of up to 1000 psia to be attained. Using various thicknesses of both copper and aluminum diaphragms, scored in a precisely controlled manner, it was possible to generate shock waves of reproducible strengths in the range $7\leq M_s\leq10$ using hydrogen, helium, their mixtures, or helium–argon mixtures as driver gases; and argon, krypton, and xenon as the driven gas. The initial driven-gas pressure could be controlled to within an error of less than 0.1 torr, to any pressure in the range $\sim$1 to 20 torr, experiments being conducted with driven pressures in a limited range of from $\sim$3 to $\sim$10 torr. A section of Pyrex tubing, 0.3 m long, was used for the microwave diagnostics. This dielectric section of tubing had, within close limits, the same internal dimensions as the aluminum tubing.

The dump tank, separated from the diagnostics section by a 0.6-m length of aluminum tubing, was used as a means of reducing the post shock-tube pressure, and was isolated from the shock tube proper by a 2-mil aluminum diaphragm. This diaphragm permitted the smaller volume of the shock tube to be treated as separate and apart from the larger dump-tank volume, and facilitated the attainment of high shock-tube purity levels.

In addition to providing a means for the generation of accurately controlled high-strength shocks, the shock tube was specifically designed to permit operation at gas impurity levels lower than those of the research-grade gases, that is, on the order of 1 ppm. Although no effort was made to improve upon the known impurity level of the research-grade gases used in these experiments, considerable effort was devoted to the reduction of the contamination of the test gases caused by outgassing from the shock-tube walls and fittings and from leakage into the tube. Prior to each run a combined outgassing and leak rate was obtained. This was accomplished by closing the gate valve to the diffusion pump (used to evacuate the shock tube to ultimate pressures in the range 2×10^{-6} to 5×10^{-6} torr) and observing the pressure read in the tube as a function of time. It was observed that the tube pressure would constantly increase to 10^{-4} torr in about 3 min and thereafter increase at a much slower rate, reaching about 2×10^{-4} torr in about 15 min. The initial pressure increase was inferred as being predominantly due to outgassing from the internal surfaces at a rate equivalent to about 1.5×10^{10} cm^{-3}·sec^{-1}.

Mass-spectroscopic analysis of the outgassing material indicated that it had an approximate composition consisting of about 60% H_2O, about 10% N_2, and about 30% hydrocarbons. To reduce the outgassing rate, the tube was heated to about 200°C while being continuously exhausted by the diffusion pump. This heating, accomplished by heating tapes wrapped around the tube, was repeated after each two or three shots.

By flowing the research-grade test gases[10] through the tube to atmosphere, it was possible to reduce the outgassing impurity level to calculated levels of fractions of 1 ppm. To preclude back diffusion of oil vapor from the roughing pump used in the flow system, a cold trap

[10] The flow rates used were equivalent to 5.8×10^{16} cm^{-3}·sec^{-1} for the 5- and 10-torr shots, and 3.3×10^{16} cm^{-3}·sec^{-1} for the 3-torr shots.

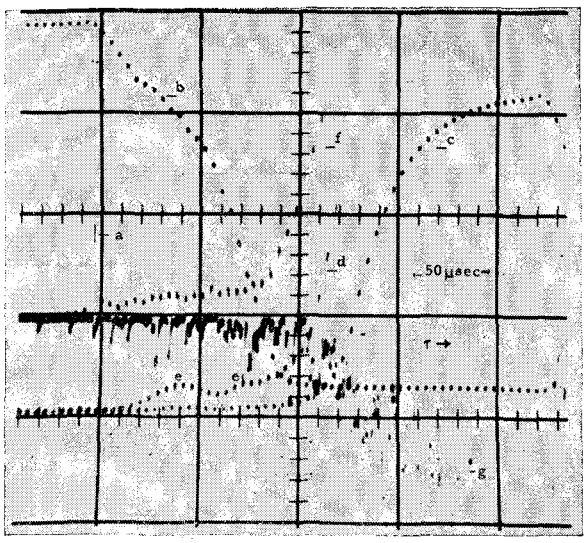

FIG. 2. Photographic enlargement of typical microwave and luminosity data. a, Estimated shock position; b, transmitted signal; c, reflected signal; d, 5-times-amplified reflected signal; e, "bumps"; f, unfiltered luminosity; g, filtered luminosity 4188 A±30 A filter).

was placed just downstream of the flow-system exit port and upstream of the pump. As a further precaution in preventing oil vapor from entering the tube during rough pumping and contributing to the outgassing process, a cold trap was provided for this line also.

SHOCK-VELOCITY MEASUREMENT SYSTEM

The small impurity level in the gases was sufficient to produce shock-front luminosity in a layer about ½-mm thick extending over the entire cross section of the tube. It was seen to be present on every luminosity profile studied; the reproduction of the test record shown in Fig. 2 shows a "light spike" from this layer at the estimated shock position. A photomultiplier shock-position indicator system was devised, employing an RCA 6655 photomultiplier tube mounted to view the shocked gas near the centerline of the tube, as a means of accurately determining shock-passage time. Four shock-position indicators, at distances of 46.1- and 26.1-cm downstream and upstream of the centerline of the microwave diagnostic system, were used to obtain information from which both shock velocity and shock attenuation could be derived.

The outputs of the shock-position indicators were amplified, differentiated, and fed to a flip-flop stage, the output of which was a pulse having an amplitude of about 7 V, a rise time of about 0.2 μsec, and a decay time of about 10 μsec. The four pips (one for each station) were then displayed on an oscilloscope raster, an example of which is reproduced as Fig. 3. This raster recording system permitted the determination of shock-passage times accurate to within 0.2 μsec over periods of time up to 2000 μsec. Mean shock velocities could usually be determined to within 0.15% accuracy. The translational temperature of the shock-heated gases was then computed from the mean-velocity data by the application of the perfect-gas equations which, for the low ionization levels encountered ($<10^{-4}$), are a quite accurate representation of the gas behavior. The shock-attenuation data were employed in analysis of the electron-density profile measurements.

MICROWAVE DIAGNOSTIC SYSTEM

The microwave circuit shown in Fig. 4 was the primary diagnostic tool in the experiment; the circuit employed a frequency of 24 GHz and was designed to monitor the amplitude of the microwave signals transmitted through and reflected from the plasma. Providing the so-called normalized effective electron collision frequency ν_c/ω is greater than approximately 0.07, the measurement of reflected and transmitted signal amplitudes provides as wide an electron-density sensitivity range as would be detected by measurement of the transmitted and reflected phases.

The measurement of signal amplitude necessitates a far less sophisticated circuit than that required for phase determination. It has been shown[11] that if the dielectric walls of the Pyrex tubing, through which the microwave beam passes, have been matched to the microwaves so that in the absence of plasma no net reflection results from the presence of the walls, then the walls will continue to be matched when plasma is present. Consequently, the presence of the Pyrex wall will not influence the characteristics of the microwave–plasma interaction. The Rexolite matching structures shown in the apertures of the transmitting and receiving horns were developed to achieve this matching. By

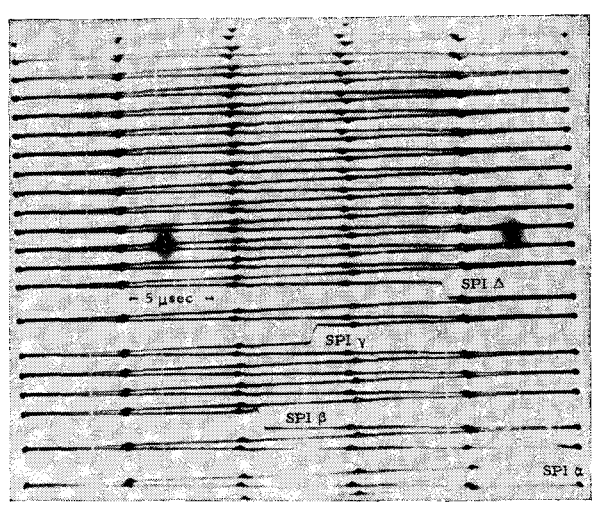

FIG. 3. Photographic enlargement of a typical oscilloscope raster.

[11] R. G. Jahn, "Interaction of Electromagnetic Waves with Slightly Ionized Gases, 1. Uniform Media," Tech. Note No. 2 Daniel and Florence Guggenheim Jet Propulsion Center, California Institute of Technology (1960).

trial and error variation of the depth and the width of the grooves machined in one surface of the structure, it was possible to match the microwave circuit to the Pyrex diagnostic section with a standing wave ratio of less than 1.05. Therefore, the Pyrex section is practically invisible to the microwaves and its presence can be neglected.

MICROWAVE-PLASMA THEORY AND CORRECTIONS

The microwave horns were of special design insofar as they collimate the microwave beam in the vertical x dimension by providing a slight degree of focusing, the output of each horn being focused on the aperture of the other. This was done in an effort to simulate, with a plasma of restricted dimensions, the theoretical case of a plane–plane-polarized monochromatic electromagnetic wave interacting with a plane slab of isotropic, homogeneous plasma whose lateral dimension is infinite in extent. This theory[12] is based on the concept of the electromagnetic wave interacting with an ensemble-averaged electron; the plasma was macroscopically characterized by the electron density N_e and the effective collision frequency ν_c of elastic momentum-exchange collisions for the electrons. This frequency usually appears in the form ν_c/ω, where ω is the microwave frequency.

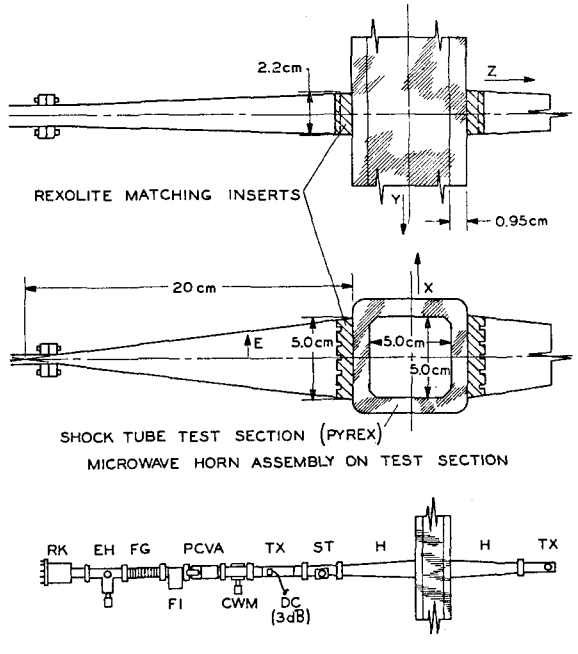

FIG. 4. Microwave diagnostic system. Nomenclature: RK, 2K50 reflex klystron; EH, E and H plane tuner; FG, flexible waveguide; FI, ferrite isolator; PCVA, precision calibrated variable attenuator; CWM, cavity wave meter; DC(3dB), 3-dB multihole directional coupler; TX, tuneable crystal mount; ST, stub tuner; H, transmitting and receiving horns.

[12] R. G. Jahn, Phys. Fluids **5**, 678 (1962).

Because the plane wave–plasma interaction theory was only partially simulated in the present experiments, a number of corrections were made to permit a more accurate interpretation of the microwave data in terms of the theory.

The fact that the microwave horns are only a few wavelengths apart, and consequently lie within each other's near field, leads to a nonuniform distribution of the microwave energy in the region where interaction with the plasma occurs. This is at variance with the concept of a plane electromagnetic wave used in the interaction theory which, by its very definition, exhibits a spatially uniform energy distribution in the direction of propagation. To account for this nonuniform energy distribution in the interpretation of results, a simplified one-dimensional model for the radial near-field pattern of the horn system was synthesized. This model correlated surprisingly well with the observed field pattern and provided a direct means for compensating for the nonuniform field. Electron densities calculated from the microwave data, with and without the application of this near-field correction factor, differed by at most 20%. However, substantial errors, on the order of 50% in ν_c/ω, could be incurred by neglecting this factor. The details of this correction are given in Ref. 13.

The microwave crystals, used to detect the transmitted and reflected signal amplitudes, did not have a linear response to incident energy. Consequently, it proved necessary to calibrate the crystal before each of the data runs as the calibration characteristics of the crystals varied slightly from day to day. Denoting the observed normalized signal amplitude as ${}_0S$ and the actual signal amplitude as ${}_1S$ as determined through use of the calibrated precision attenuator, the empirical relationship, Eq. (3), was found to be a quite accurate representation of the calibration data

$$ {}_1S = A({}_0S)^K. \tag{3}$$

The exponential factor K had a value of between 0.85 and 1.30, a value of unity corresponding to a square-law detector.

The effect of the electron-density boundary layer, in particular the gradient in the direction of propagation, upon the microwave measurement of plasma properties has been investigated[14] and found to be unimportant for the operating regimes of interest. A qualitative investigation of the effects of the electron-density gradient normal to the direction of microwave propagation leads to the conclusion that at the highest Mach numbers attainable, where a significant variation in electron density can exist over the dimensions of the

[13] A. J. Kelly, "Atom-Atom Ionization Mechanism and Cross Sections in Noble Gases and Noble Gas Mixtures" Ph.D. thesis, California Institute of Technology, Pasadena, Calif., 1965.

[14] F. A. Albini and R. G. Jahn, J. Appl. Phys. **32**, 75 (1961).

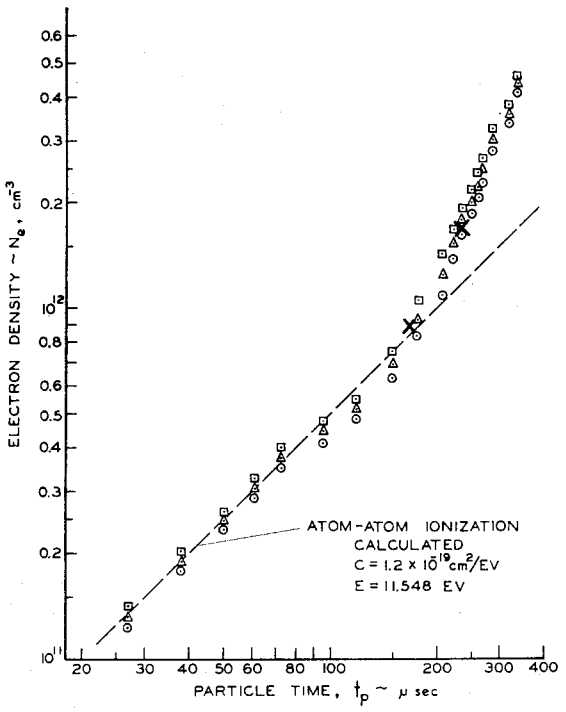

FIG. 5. Electron density vs particle time, Run No. 945. Argon, 3 torr, $\beta=1.386$. ×, Hybrid-phase ("bump") data; ⊡, $\nu_c/\omega=0.07$; △, $\nu_c/\omega=0.08$; ⊙, $\nu_c/\omega=0.09$.

field pattern, the microwave system will indicate electron-generation rates lower than the true values.

INTERPRETATION OF MICROWAVE DATA

An IBM computer program was developed to facilitate the accurate, rapid interpretation of the microwave data, taking into account the field-pattern and crystal-correction factors.

The input to the program consisted of the transmitted signal from the oscilloscope (e.g., Fig. 2), an assumed value of ν_c/ω, the crystal-correction, the field-pattern correction, and the physical parameters of the experiment. The electron density was computed using the microwave–plasma interaction theory discussed earlier.

The data of Fig. 2 yield the results shown in Fig. 5, where the calculated electron density N_e is plotted as a function of particle time t_p for various values of ν_c/ω.

The simplified theory used to describe the electromagnetic-wave–plasma interaction characterized the plasma by the electron density and the electron-heavy particle collision frequency ν_c. Consequently, two independent measurements of the electromagnetic-wave interaction with the plasma are required to determine these two parameters unambiguously. Accordingly, two measurements were made, the transmitted and reflected signal amplitudes. However, the process of matching the transmitted and reflected signal data led to a considerable degree of uncertainty in the determination of ν_c/ω, and therefore in the electron-generation rate. The use of data from the transmitted signal data and the so-called hybrid phase or "bump" lead to a more satisfactory method of determining ν_c/ω.

Jahn[8] observed that by producing a small mismatch in the stub tuner of the microwave circuit (Fig. 4), bucking this signal out by adjusting the stub of the transmitted-signal crystal mount so that in the absence of a plasma the reflected signal was negligible, the circuit produced small-amplitude reflected signals in the manner of an interferometer. These signals appear on the reproduced test record of Fig. 2 as a small-amplitude oscillation of the 5-times-amplified reflected signal. An analysis of the hybrid-phase process[13] shows that these data, corresponding to the extrema of the oscillatory trace, are relatively weak functions of ν_c/ω. Referring back to Fig. 5, we see that the hybrid-phase measurement provides an unambiguous determination of ν_c/ω. The collision frequency ν_c can be interpreted in terms of an electron-heavy particle elastic momentum-exchange collision process and provides a means by which the validity of the simplified microwave-plasma theory can be evaluated.

Once ν_c/ω has been determined, it is possible to plot the electron density versus particle time and to determine the initial slope which characterizes the atom–atom ionization process. For the example shown, the determination of the initial slope is a trivial matter; the initial portion of the trace is linear, indicating that the effects of shock attenuation upon the electron-generation rate are negligible. For cases where the particle times are longer and/or the shock-attenuation factor is larger, the electron density exhibits a con-

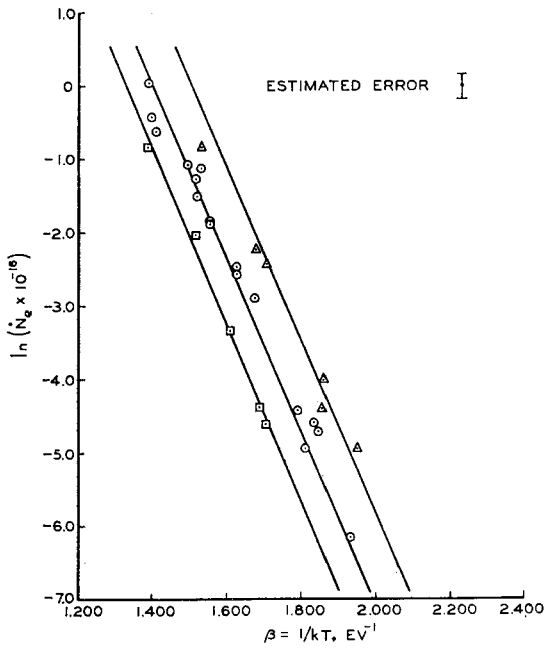

FIG. 6. Arrhenius plot for ionization of argon. ⊡, 3 torr, $N=4.41\times10^{17}$ cm^{-3}; ⊙, 5 torr, $N=6.96\times10^{17}$ cm^{-3}; △, 10 torr, $N=13.26\times10^{17}$ cm^{-3}. Calculated using $C=1.2\times10^{-19}$ cm^2/eV and $E=11.548$ eV.

tinuous, monotonic increase with time, no portion of the trace being linear. This behavior is caused by variations in the shock speed; the shock weakens as it passes along the tube so that the gas temperature will increase with time when viewed in laboratory coordinates. This effect is discussed in detail in Ref. 13. Knowledge of the attenuation factor permits an observed electron-density trace, influenced by shock attenuation, to be reduced to an equivalent constant-temperature experiment. In other words, it compensates for the attenuation-induced temperature variation within the body of the gas.

Once the initial slope, corresponding to the atom–atom generation rate, has been determined, a minor normalization correction is applied. This correction, never exceeding 5%, compensates for the small variations of neutral-particle density resulting from variations in the initial pressure or temperature of the shocked gas. Quadratic density dependence of the atom–atom two-step ionization is assumed to hold for this correction. Thus reduced, the electron-generation data are in a form suitable for presentation on an Arrhenius plot, for example, those shown in Figs. 6 through 8.

RESULTS

Ionization Cross Sections

Following the data reduction procedures outlined above, the Arrhenius plots for the pure gases, argon

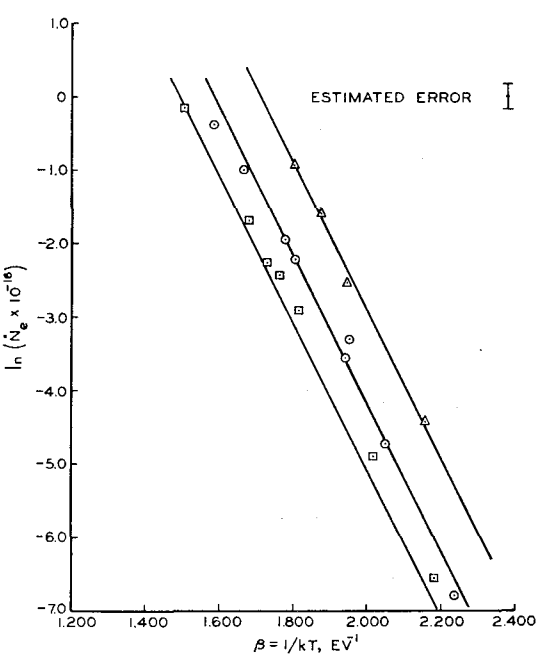

FIG. 7. Arrhenius plot for ionization of krypton. ⊡, 3 torr, $N=4.41\times10^{17}$ cm^{-3}; ⊙, 5 torr, $N=6.96\times10^{17}$ cm^{-3}; △, 10 torr, $N=13.26\times10^{17}$ cm^{-3}. Calculated using $C=1.4\times10^{-19}$ cm^2/eV and $E=9.915$ eV.

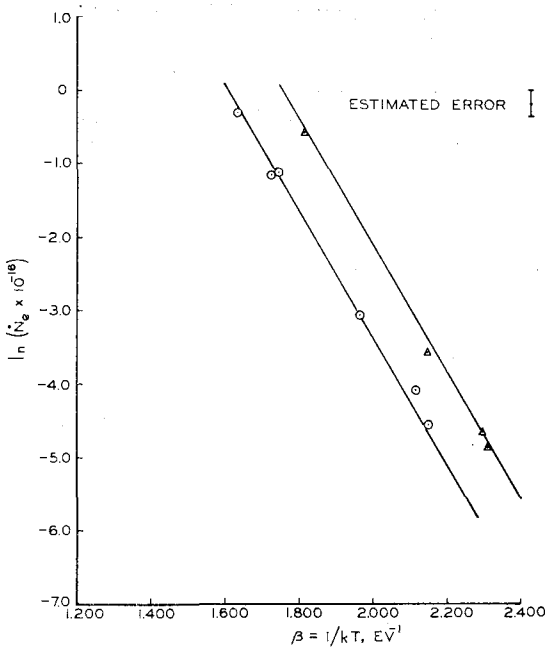

FIG. 8. Arrhenius plot for ionization of xenon. ⊙, 5 torr, $N=6.96\times10^{17}$ cm^{-3}; △, 10 torr, $N=13.26\times10^{17}$ cm^{-3}. Calculated using $C=1.8\times10^{-20}$ cm^2/eV and $E=8.315$ eV.

(Fig. 6), krypton (Fig. 7), and xenon (Fig. 8), were developed. The error brackets shown in these figures represent what is considered to be a reasonable estimate of the uncertainty involved in the determination of the initial slope of the electron-generation-rate curve, around ±20%, and those errors in calculated atom temperature resulting from uncertainty of the shock velocity. The effects of lateral electron-density gradients are not included in the error estimate quoted. This phenonemon, which becomes significant at high Mach numbers and low values of β, tends to depress the initial electron-generation rate below its true value. As a sequence, the data taken at low values of β fall consistently below the curve representative of the best fit to the data.

The activation energies and cross-sectional slope constants derived from the data of Figs. 6, 7, and 8 are presented in Table I. The magnitude of the error brackets associated with the data on the Arrhenius plots introduces some uncertainty in determining the line best fitting the data. The uncertainties in E_* shown in the table are representative of the maximum slope variations that the data would allow. These variations amounted to less than 10% of the mean value in all instances. Moreover, the mean values of the excitation energies are each within 0.4 eV of the lowest metastable levels listed by Cook.[15] The close correlation between each experimentally determined activation energy and the corresponding lowest metastable excited state supports the contention that

[15] *Argon, Helium, and the Rare Gases*, G. A. Cook, Ed. (Interscience Publishers, Inc., New York, 1961), Vol. 1.

TABLE II. Cross-sectional slope constants.

Species	C
Argon	1.2×10^{-19} cm²/eV±15%
Krypton	1.4×10^{-19} cm²/eV±15%
Xenon	1.8×10^{-20} cm²/eV±15%

ionization proceeds in *two* steps, the first step being rate controlling. This is consistent with the work of Harwell and Jahn.[8] From the work of Ecker and Kröll,[16] it is inferred that the apparent excitation energy is lowered, due to the presence of microfields in the plasma, by less than 0.01 eV, an amount which is insignificant in comparison with the experimental error.

A least-squares curve-fitting IBM 7090 computer program was devised for the purpose of providing an unprejudiced means of interpreting the data of the Arrhenius plots. The theoretical atom–atom ionization-rate equation [Eq. (2)] was fitted to the data points with minimum error. This fit is accomplished by varying the cross-sectional slope constant (C), the activation energy (E_*) being fixed and specified as input to the program. For the values shown in the table, the activation energy was chosen to be equal to the first metastable energy level, in accordance with the concept of a two-step excitation–ionization process.

The cross-sectional slope constants (C) are within a scatter of 15%, independent of the neutral-particle-density level, i.e., independent of the pressure level. Inasmuch as the data were reduced using the theoretical atom–atom electron-generation-rate equation, where the generation rate is quadratic in neutral-particle density, it can be stated that the quadratic pressure dependence of the atom–atom two-step ionization process has been substantiated. To put the 15% scatter into proper perspective, it should be realized that if we take as unity the number of electrons generated at a particle-density equivalent to 3 torr (4.414×10^{17} cm^{-3} in this case) and a fixed temperature T, then at 5 torr the electron generation rate would be $\sim2\frac{1}{2}$, and at 10 torr approximately 9, or almost an order-of-magnitude variation due to pressure effects.

Weighing the cross-sectional slope constants (C) according to the number of data points available at each pressure results in the following values for the three noble gases tested.

The most singular aspect of the cross-sectional slope constant data presented in Table II is that the C factor for xenon appears to be an order of magnitude smaller than would be expected from the data for argon and krypton. In the absence of a complete theory of the atom–atom excitation–ionization process, or even a detailed mechanism, any attempt to explain the relatively diminuitive size of the xenon cross-sectional slope seems excessively speculative. It would be equally speculative to try to explain why the argon and krypton slope constants are, to within experimental error, equal.

At values of $\beta\gtrsim 2.0$, i.e., at low temperatures, the behavior of pure xenon during the initial ionization phase was conspicuously different than that of argon and krypton. The difference appears as a pronounced increase in electron density to a level between 10^{11} and 2×10^{11} cm^{-3} immediately[17] after the passage of the shock. This initial electron-density rise was observed to be almost linear and was followed by what appears to be a normal atom–atom two-step ionization process. The atom–atom electron-generation-rate data were computed by first subtracting out this initial "block" of electron density, the results correlating remarkably well with data taken at higher Mach numbers (low β) where this "pre-ionization" phenomenon was not evident.

For temperatures corresponding to $\beta>2.4$, the atom–atom phase was so weak that no useful data could be collected. The times involved in this sharp rise in electron density were too long for it to be related to the preliminary phases of the atom–atom ionization process. Photoionization seems highly improbable because visible luminosity was almost completely lacking in all pure gas runs and because of radiation trapping. It is possible that an impurity, perhaps water vapor, is ionized, and rapidly attains an equilibrium level of ionization. This level, around 2×10^{11} cm^{-3}, would correspond to an impurity level of about 2×10^{-7} if the impurity were completely ionized. This is of the same order as the calculated "uncontrolled" impurity level of the shock tube. However, it should be re-emphasized that while the uncontrolled impurity level was, as far as can be determined, consistent from run to run, this behavior was peculiar to the xenon tested and bears further study.

ELECTRON-ATOM ELASTIC-MOMENTUM-EXCHANGE CROSS SECTION

By matching the transmitted signal amplitude to the hybrid phase (bump) extrema, it is possible to determine both the electron density and the effective collision frequency ν_c. From the simplified interaction theory, the collision frequency ν_c can be written as

$$\nu_c=\sum_j N_j\langle vQ_{dj}\rangle,$$

where N_j is the particle density of the atoms and ions in the plasma and $\langle vQ_{dj}\rangle$ is the product of the electron velocity and the monoergic beam cross section for elastic momentum exchange, averaged over the electrons' velocity distribution. Since the approximate[18]

[16] G. Ecker and W. Kröll, Phys. Fluids **6**, 62 (1963).

[17] In times of 100–200 μsec compared with useful electron-density-data test times of ~2000 μsec.

[18] ν_c is considered to be a constant, i.e., $\nu_c\neq\nu_c(T_e)$.

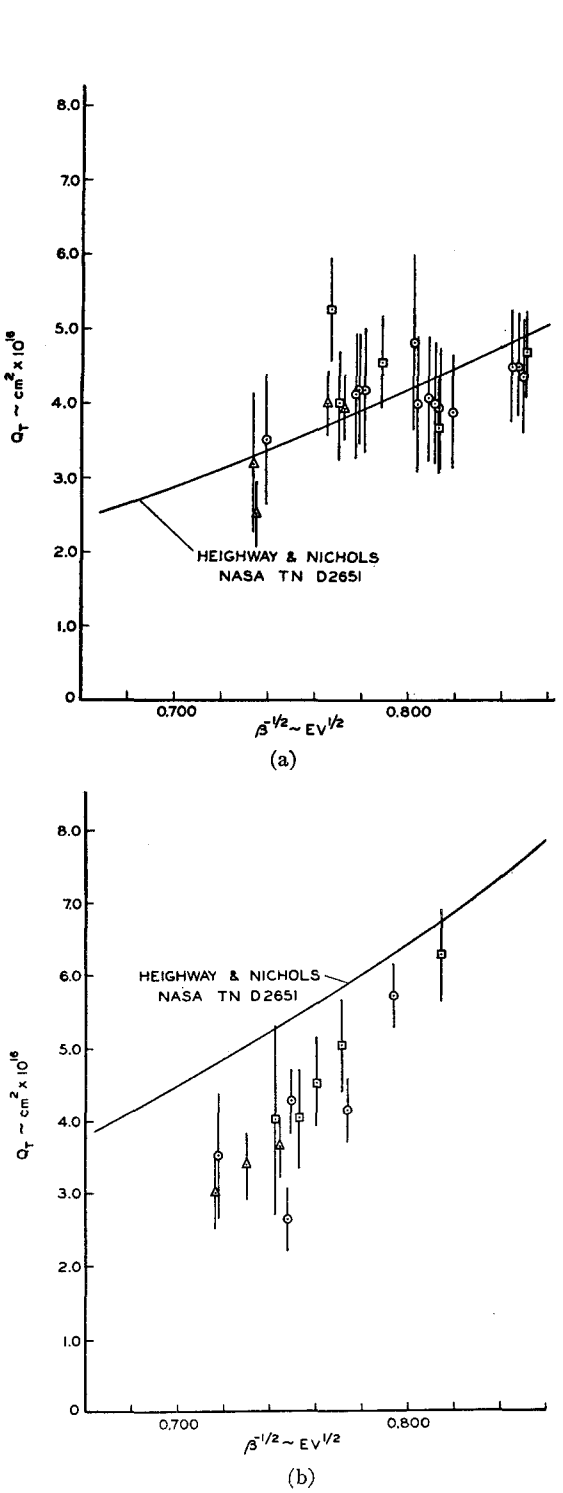

FIG. 9. (a) Q_T versus $\beta^{-\frac{1}{2}}$ for argon. ⊡, 3-torr data; ⊙, 5-torr data; △, 10-torr data. Electron and atom temperature assumed equal. (b) Q_T versus $\beta^{-\frac{1}{2}}$ for krypton. ⊡, 3-torr data; ⊙, 5-torr data; △, 10-torr data. Electron and atom temperatures assumed equal. (c) Q_T versus $\beta^{-\frac{1}{2}}$ for xenon. ⊙, 5-torr data; △, 10-torr data. Electron and atom temperature assumed equal.

microwave interaction theory was based on the concept of the ensemble-averaged electron, the following representation of ν_c was used to correlate the data and should be consistent with the basic theory:

$$\nu_c = N\bar{v}_e Q_T,$$

where $\bar{v}_e$ is the mean electron velocity, i.e., $(8kT_e/\pi m_e)^{1/2}$, m_e and T_e the mass and temperature of the electron, and Q_T the "total" elastic electron-momentum-exchange cross section. The first hybrid-phase maxima, occurring at an electron density of around 0.9×10^{12} cm^{-3}, was employed as the primary determination of

ν_c/ω; subsequent hybrid extrema were used to improve the accuracy of determining this parameter. Using Spitzer's[19] cross section for Coulombic elastic momentum exchange, calculated values of ν_c/ω are less than 10^{-3} in the appropriate range of temperatures and electron density. The observed values of ν_c/ω, however, ranged from 0.05 to about 0.25, so that Q_T can be identified with the electron–atom elastic cross section, other contributions accounting for less than 1% of the total.

The experimentally determined values of Q_T are presented for pure argon, krypton, and xenon in Figs. 9(a) through 9(c), respectively, as functions of $\beta^{-1/2}$. Their calculation employs the assumption that the electron and atom temperatures were equal, that is, $T_e=T_a$ and $\beta=1/kT_a=1/kT_e$, where T_e and T_a are, respectively, the electron and atom temperatures. Since $\bar{v}_e=(8kT_e/\pi m_e)^{1/2}$, $\beta^{-1/2}$ is then directly proportional to the mean electron velocity. Comparing traces of electron density versus time for argon with computed electron-density profiles using the known atom–atom and electron–atom ionization cross sections,[20] indicates that the difference between the electron and atom temperatures (T_a-T_e) reaches a maximum of $\sim$500°K at an electron density of about 1.2×10^{12} cm^{-3}, i.e., between the first hybrid-phase maxima and the first minima. At electron densities greater than 3×10^{12} or lower than 0.4×10^{12}, the electron and atom temperatures were found to be equal $(T_a=T_e)$ to within experimental error. Therefore, when plotted as a function of $\beta^{-1/2}$ $(T_e=T_a)$, the values for Q_T are somewhat lower and shifted to somewhat higher values of $\beta^{-1/2}$ than is actually the case if T_e rather than T_a were used to compute $\beta^{-1/2}$. The error brackets accompanying the data are indicative of the uncertainties involved in matching the hybrid phase and the transmitted signal data.

The results computed by Heighway and Nichol,[21] through Maxwell averaging the beam cross-sectional data compiled by Brown,[22] are also presented in Figs. 9(a)–9(c). These results, denoted "Heighway, Nichols NASA TN D-2651" on the graphs, exhibit good agreement with the results from microwave experiment data. The agreement is particularly good in the case of argon, virtually all of the microwave data falling within ±20% of the curve. Good agreement is also shown for krypton. The xenon microwave data is, at low values of $\beta^{-1/2}$, a trifle less than a factor of 2 lower than the beam data, the disparity decreasing to $\sim$30% at high $\beta^{-1/2}$ values. This discrepancy corresponds to an electron temperature $\sim$1000°K less than the atom temperature. The beam data have associated with them an uncertainty which, although not stated, probably is of the order of ±10%.[23] A remarkable aspect of the apparent close agreement is the fact that the microwave theory employs an equation of motion for the electron which assumes that ν_c is independent of electron velocity and therefore temperature. This may contribute to the better agreement of the microwave and beam data for argon, where the Maxwell-averaged elastic-momentum-exchange cross section is a relatively weak function of temperature, in contrast with the poorer correlation exhibited by xenon and krypton, whose Maxwell-averaged elastic momentum-exchange cross sections are somewhat more temperature dependent.

[19] L. Spitzer, Jr., *Physics of Fully Ionized Gases*, Interscience Tracts on Physics and Astronomy, No. 3 (Interscience Publishers, Inc., New York, 1956).

[20] An electron–atom (argon) inelastic (ionization) cross-sectional slope constant equal to 7×10^{-18} cm^2/eV was employed for these calculations, cf. Ref. 1.

[21] J. E. Heighway and L. D. Nichols, "Brayton Cycle MHD Power Generation with Non-Equilibrium Conductivity," Natl. Aeron. Space Admin. Tech. Note D-2651 (1965).

[22] S. C. Brown, *Basic Data of Plasma Physics* (Tech. Press, Cambridge, Mass. and John Wiley & Sons, Inc., New York, 1959).

[23] E. W. McDaniel, *Collision Phenomena in Ionized Gases* (John Wiley & Sons, Inc., New York, 1964).